International Journal on Interactive Design and Manufacturing (IJIDeM)
https://doi.org/10.1007/s12008-023-01439-w

ORIGINAL PAPER

Modeling and optimization of bead geometry and hardness of bead on plate TIG welds of Stainless Steel SS202

Anand Baghel[1] · Chaitanya Sharma[2] · Manvandra Kumar Singh[1] · Vikas Upadhyay[3]

Received: 2 January 2023 / Accepted: 30 June 2023

Abstract
The quality and load-carrying capacity of weldments mainly depends on selecting suitable levels of input welding parameters. Current research intends to optimize input parameters, viz. current and welding speed, for various weld characteristics like penetration depth, weld width, weld bead hardness, and HAZ hardness for tungsten inert gas welded SS202. Experiments were organized using the response surface methodology's central composite face-centered design approach. The experimental findings were analyzed using ANOVA, and regression equations were developed for all output parameters. Higher current and slower welding speeds increase penetration depth and weld width, and vice versa. The greatest penetration depth (1.764 mm), minimum weld width (4.097 mm), maximum weld bead hardness (347 Hv), and heat-affected zone hardness (302 Hv) were achieved with the optimized input values of welding current and speed, which were 103 A and 5 mm/sec, respectively. A confirmation test revealed that the predicted values aligned well with experimental results.

Keywords Response surface methodology · Stainless steel · Tungsten inert gas welding · Multi-objective optimization · Depth of penetration · Weld width · Hardness

1 Introduction

Steel is the structural material that is most frequently utilized in a variety of engineering applications. SS202 possesses many advantageous characteristics, such as good formability, moderate tensile strength, resistance to solidification cracking, improved ductility, and excellent weldability arising from adding chromium and nickel with low carbon content [1]. Due to its advantageous cost and desirable properties, SS202 is frequently used to create permanent leak-proof joints for numerous applications in automotive, chemical, food processing, nuclear power plants, tubes for boilers, railway coach building, etc. [2]. Various joining techniques are available for welding different ferrous and non-ferrous materials, such as different-grade steels, aluminum, etc. These techniques include tungsten inert gas (TIG) welding, metal inert gas (MIG) welding, cold metal transfer welding, friction stir welding (FSW), plasma welding, and laser welding etc. [3–6]. TIG welding is one of the innovative techniques capable of welding thin and thick sheets of various materials, including aluminum, copper, stainless steel, high strength low alloy steels, etc., in similar and dissimilar combinations with or without filler material. It offers superior process control, accuracy, better weld quality, and characteristics at low cost over other techniques like shielded metal arc welding and metal inert gas welding; therefore, it is more frequently used to weld not only SS202 but also other steels [7].

The success of the welding process is attributed to its ability to produce welds of superior quality at a reduced cost, which is, in turn, managed by the optimization of process parameters. Independent parameters dominate weld quality and characteristics, viz., welding current, voltage, welding speed, arc gap, shielding gas type and flow rate, groove geometry, torch angle, wire feed rate, etc. Output parameters like weld bead geometry, electrode melting rate, depth of penetration (DOP), heat affected zone (HAZ) size, base metal melting rate, weld hardness, and tensile strength, etc., all are affected by independent input parameters, therefore,

✉ Chaitanya Sharma
chaitanya.sharmaji@gmail.com

[1] Department of Mechanical Engineering, Amity University Madhya Pradesh, Gwalior, India

[2] Department of Mechanical Engineering BIT Sindri, Dhanbad, India

[3] National Institute of Technology Patna, Patna, India

Published online: 14 July 2023

need to be selected and controlled carefully. Statistical optimization approaches such as desirability analysis, grey based Taguchi helps to find out multi-objective optimization accurately; however, artificial intelligence techniques predict outcomes more precisely than traditional methods and can manage numerous parameters simultaneously [8].

Heat input to weld, weld thermal cycle, and peak temperature all are greatly affected by process parameters which in turn are accountable for weld flaws, macrostructure, and microstructure, as well as mechanical (strength, hardness, ductility) and other qualities, all determined by these process parameters [9]. Welding current and speed decide the heat input per unit weld length and peak temperature [10]. A faster welding rate means that welding arch will spend less time at a location, hence less heat input and low peak temperature resulting in a thin and shallow weld bead, i.e., less penetration and reinforcing. Low welding speeds result in high heat input and peak temperature; therefore, wide and thick weld beads with excessive reinforcement. Low current results in a narrow bead with a small depth of penetration and difficulty in initiating the arc. However, excessive current causes a wider, flattened weld bead, greater penetration levels, a larger HAZ, increased angular distortion, and an uneven bead profile [11].

Input parameters, namely welding current, shielding gas and its flow rate, electrode diameter, and groove angle, were planned using the design of an experiment for TIG welding of SS202 for a 6 mm thick plate. Welding current was reported as the most important input parameter influencing tensile strength and weld hardness. Electrode diameter influenced weld tensile strength significantly but didn't significantly affect the hardness. The weld hardness diminishes significantly when the welding current changes from 160 to 240 A. Moreover, different groove angles, shielding gases, and flow rates do not influence weld tensile strength and hardness. The optimal parameters were 240 A, 14 V, and 25 l/min, resulted in the highest weld hardness at the fusion zone of 297.3 Hv [12]. Welding speed was reported to be a more important parameter than the welding current and filler diameter [13]. Optimal welding parameters, viz. current, welding speed, gas flow rate, and filler rod for single pass butt welding of 4.75 mm thick SS304, were obtained using the Taguchi technique. High heat input at 180 A current deteriorates the grain structure and diminishes the weld hardness to 92 Hv, whereas 150 A gives a maximum hardness of 100 Hv [14]. The welding speed and current had the greatest impact on the tensile strength and hardness of the Al6061/Al5083 TIG welded dissimilar joints. In addition, non-optimal input parameters resulted in low weld hardness and tensile strength due to greater degree of softening and coarsening and larger HAZ, porosity, voids, and other flaws [15]. TIG offered a coarse dendritic grain structure and inferior mechanical properties of AA7039 welds than FSW. Tensile strength, hardness, and ductility were all seriously lower than base metal [16].

DOP can be improved by increasing current and decreasing welding speed and arc gap, resulting in a bigger weld bead and HAZ. Accordingly, the current need to be carefully regulated for each plate thickness and material type [17]. An innovative, effective, low-cost way to raise the DOP with a reduced weld width is to use activated fluxes while welding on the weld surface. Oxide, chloride, and base fluxes are commonly used in TIG welding to enhance weld bead geometry as per material composition. TIG welding with activated fluxes is commonly known as A-TIG and can easily join gauge sections up to 12 mm thick in a single pass [18]. Specifically, reverse Marangoni convection and arc constriction are to blame to yield deep and narrow weld penetration, i.e., thin HAZ. Al_2O_3, SiO_2, TiO_2, and their hybrid mixture reasonably enhanced the DOP without increasing weld width while welding SS304 plates of 4 to 8 mm thickness [19]. Compared to other carbonated fluxes used for bead-on-plate welding of 6 mm thick AISI 1018, the borax flux produced a greater depth of penetration and a higher aspect ratio [20]. For dissimilar welding of 3 mm thick plates of SS304 and SS202 without filler material, the use of oxide flux yielded complete weld penetration, while chloride flux did not [21].

According to the literature review, there is insufficient research on multi-response optimization using RSM for TIG-welded SS202, where welding current and speed are the most important determining factors. Therefore, the present research focuses on optimizing input parameters, namely, current and welding speed for bead-on-plate TIG welding of SS202, taking into account multi-response optimization (DOP, weld width, weld bead hardness, and HAZ hardness) utilizing the central composite design (CCD) approach and investigating their influence on weld characteristics like bead profile, weld microstructure, weld size and weld bead hardness and HAZ hardness to enhance weld quality and productivity at low cost.

2 Materials and experimental methods

2.1 Material

Stainless steel SS202 plates with 100 mm × 70 mm × 5 mm dimensions were used as the base metal in the current investigation. SS202's nominal chemical composition is listed in Table 1. After hand grinding, acetone was used to completely clean the plates' surfaces to eliminate contaminants like dirt and grease.

Table 1 Chemical composition of SS202 (wt%)

Material	C	Cr	Mn	Cu	Ni	N	Si	Mo	S	P	B	Fe
SS202	0.048	16.10	7.40	1.64	4.04	0.106	0.40	0.194	0.001	0.027	0.003	Bal.

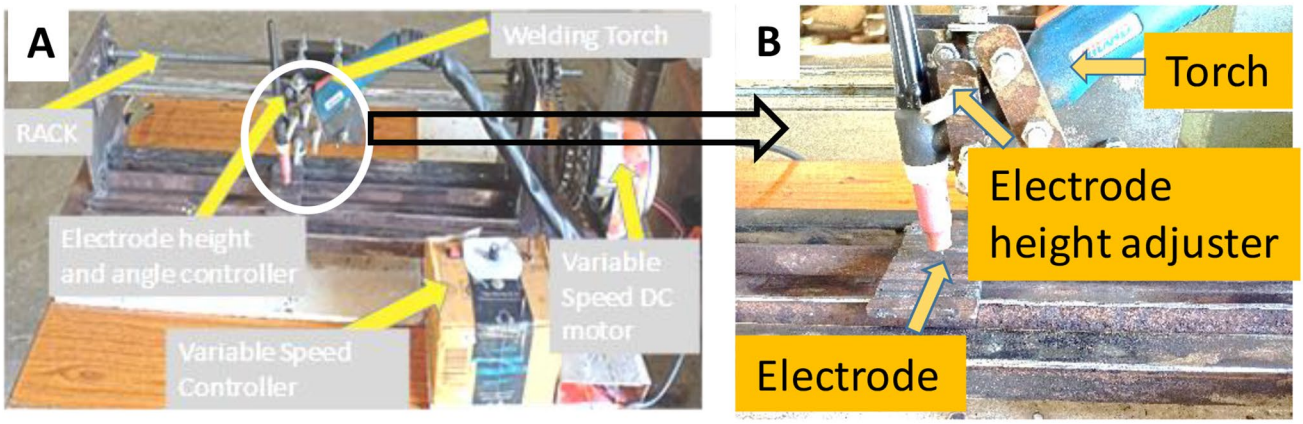

Fig. 1 Setup for (**a**) Constant feed and arc controller (**b**) Electrode height and angle controller

Table 2 Fixed parameters

Shielding Gas	Voltage	Material	Arc Gap	Electrode Diameter	Electrode Included Angle	Power Source
Argon, 13 lpm	20 V	SS-302	2 mm	2.3 mm	15° (Sharp pointed)	DCEN

2.2 Welding setup

The air-cooled TIG welding machine was used for a bead on plate welding. Argon and thoriated tungsten were employed as shielding gas and electrode for welding, respectively. Many pilot studies were carried out to identify a range of process parameters. During pilot testing, currents less than 80 A did not penetrate, while currents greater than 120 A melted the 5 mm thick plate, resulting in a current range of 80 to 120 A, yielding good welding. C-clamps were used to keep the plates aligned on the welding table and prevent plate distortion due to variations in the cooling rate. A steady supply of industrial argon gas at 13 l/min was used for the experiments.

2.3 Constant feed and arc gap control setup

Maintaining welding speed and arc gap constant is difficult in manual welding and causes variations in heat input and melting rate. Thus, precise control of welding speed and arc gap is essential, to achieve weld with uniform beads and quality. An indigenous setup, as shown in Fig. 1, was created to produce linear autogenous weldments with constant feed and arc gaps.

This welding setup has a 250 A power source with a variable current setting option. A DC motor with a variable speed control was used to supply variable speeds to the welding torch. As illustrated in Fig. 1a, the variable speed motor powers the chain and sprocket arrangement. It offers variable speed to move the welding torch on the stationary plate of base material according to the need of experimentation. Welding speed was kept constant using a speed controller coupled to a DC motor to ensure a consistent weld bead with high reproducibility. An arc gap of 2 mm was maintained throughout the experimentation using an electrode height adjuster from the workpiece, as illustrated in Fig. 1b.

2.4 Methodology

Pilot trials were first carried out on base metal to ensure defect-free bead-on-plate welds of 70 mm length utilizing selected input parameters. Following these tests, it was determined to maintain fixed values for shielding gas type, gas flow rate, arc gap, and electrode diameter, as shown in Table 2. The primary experiments were carried out by altering the current and welding speed while holding the other parameters constant. Experiments were conducted according to the CCD approach of RSM, with two variable parameters at three levels (-1, 0, + 1), as listed in Table 3. Nine distinct experiments and four replications of the central value of the input parameters were carried out, comprising a total of 13 experiments. The replication experiments conducted at the center value of the input parameters aid in achieving greater accuracy for the experimental and statistical analysis.

After bead-on-plate welding, the test samples were cut with a hacksaw at a low cutting speed to avoid any change

Table 3 Variable process parameters and their levels

S. No.	Parameters	Units	Symbols	Levels		
				-1	0	1
1	Welding Current	A	I	80	100	120
2	Welding Speed	mm/sec	S	3	4	5

Table 4 Centre composite design for TIG welding along with multi-responses

Std	Run	Current (A)	Welding speed (mm/sec)	DOP (mm)	Weld Width (mm)	Weld Bead Hardness (Hv)	HAZ Hardness (Hv)
5	1	80	4	1.37	3.71	315	311
7	2	100	3	2.12	4.57	311	307
4	3	120	5	2.2	4.73	324	290
1	4	80	3	1.78	3.74	304	317
8	5	100	5	1.7	3.84	346	301
3	6	80	5	1.22	3.21	341	300
2	7	120	3	2.48	5.11	295	280
9	8	100	4	1.7	4.17	329	304
11	9	100	4	1.8	4.21	325	304
12	10	100	4	1.63	4.25	326	305
10	11	100	4	1.7	4.64	326	304
6	12	120	4	2.31	4.98	300	283
13	13	100	4	1.7	4.24	327	303

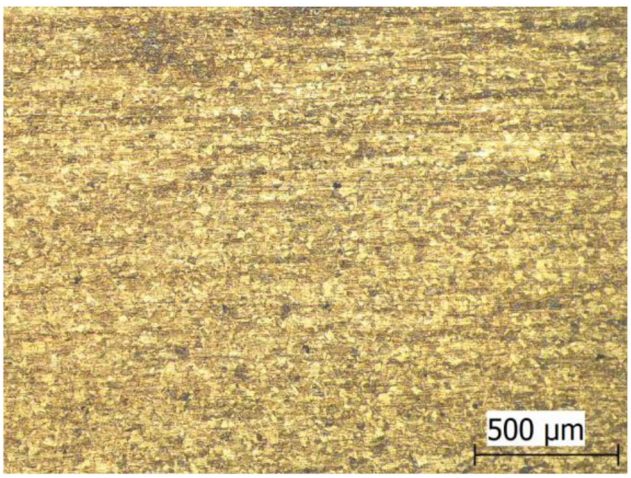

Fig. 2 Microstructure of base metal SS202

in HAZ. Standard metallography procedures were used to cold mount and polish cut samples (10 mm × 8 mm). The optical microscope was used to study the HAZ width and the evolution of the microstructure resulting from welding. The hardness of various zones of bead on plate welds was tested using a Vicker hardness tester. The input parameter set and corresponding (obtained) response parameters (DOP, weld width, weld bead hardness, and HAZ hardness) are presented in Table 4.

3 Results and discussion

3.1 Microstructure

The microstructure of as received SS202 is displayed in Fig. 2. Grains were equiaxed and aligned to the rolling direction.

The selected welding parameters resulted in proper weld beads; they were free from any visible welding defects, and zone characteristics to fusion welding are also clearly seen; however, they influenced weld bead shape, DOP, and width, as evidenced from the microstructure shown in Fig. 3. DOP increased as the welding current increased but decreased as the welding speed increased. While increasing welding speed at a constant current causes the weld width to decrease, the opposite is true when increasing the welding current. Lower heat input per unit weld length is achieved with faster welding speeds, limiting weld width and penetration, resulting in a lower DOP than other welds. On the other hand, increased current at constant welding speed increases heat input to weld, resulting in deeper penetration and higher DOP. Faster welding speed and higher welding current limit weld width and improve DOP, resulting in a higher aspect ratio.

Variation in bead shape, i.e., DOP and width with process parameters, also affects the microstructure and mechanical properties of the welded materials. Weld width decreases by up to 50% as welding speed increases, as does penetration depth. When increasing the current

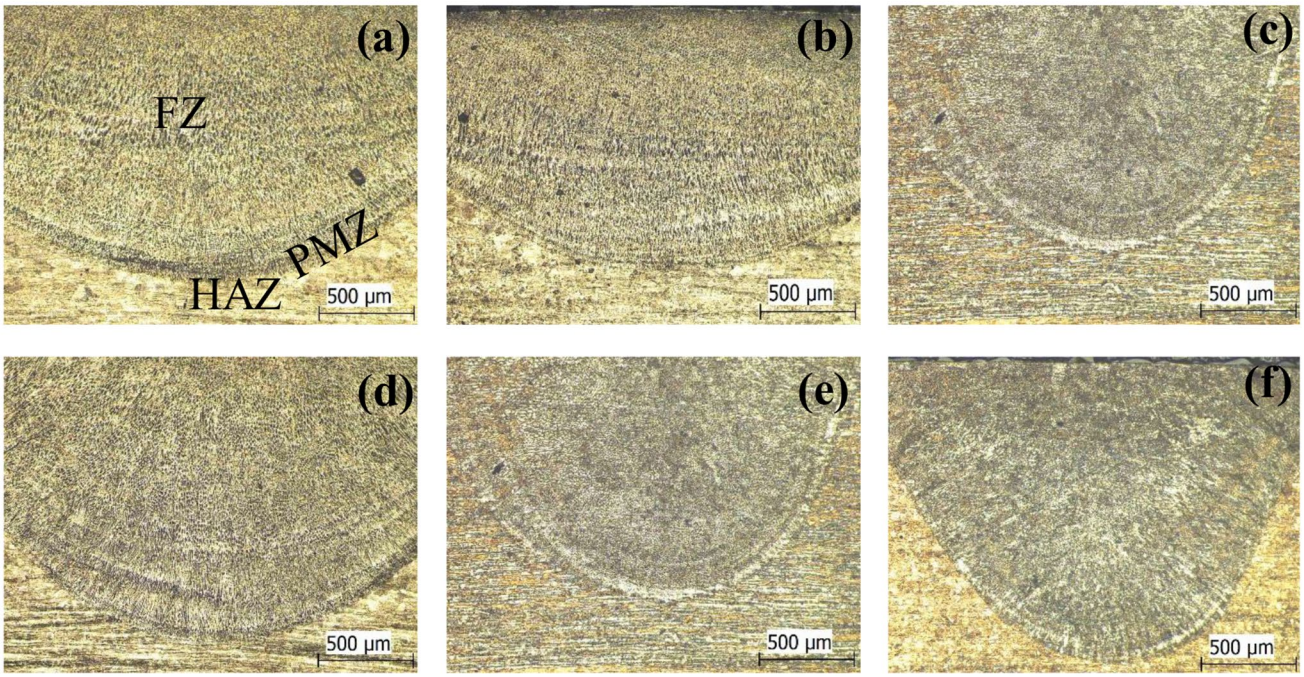

Fig. 3 Influence of welding parameter on microstructure; welding speed of (**a**) 3 mm/sec, (**b**) 4 mm/sec, and (**c**) 5 mm/sec at a constant current of 100 A and welding current (**d**) 80 A, (**e**)100 A and (**f**) 120 A at a constant welding speed of 5 mm/sec

from 80 to 120 A, the depth of penetration and weld bead width increase, as illustrated in Fig. 3.

3.2 Model development and statistical analysis

Design-Expert Software was used in this work for model development and statistical analysis. Models were selected based on the sum of squares, lack of fit, and model summary statistics. The selected model should maximize adjusted R^2 and predicted R^2 and should have an insignificant lack of fit. So, the linear model was selected for weld width, whereas the quadratic model was selected for the remaining responses. The developed models were analyzed with ANOVA, and their R-Square statistics were determined. The impact of the input process factors at three levels was investigated on each of the four responses using ANOVA tables. The ratio of the mean square value of the model to the mean square value of the residual yields the model's F value. The significance of the parameters was determined with the help of the P-value. If the P-value is less than 0.05, the input parameter is statistically significant at a 95% confidence level. Otherwise, the term is insignificant and may be removed from the regression model. The R^2 score indicates how much of the variability in the data is explained by the ANOVA model [22].

3.2.1 Depth of penetration (DOP)

ANOVA for DOP is presented in Table 5, which shows that the terms A, B, and B^2 are significant model terms. Also, the P value for the lack of fit is greater than 0.05, hence insignificant. The current contribution dominates with 72.61%, whereas welding speed contributes 16.85% to the DOP. The predicted R^2 of 0.9186 is in reasonable agreement with the adjusted R^2 of 0.9687, whereas the adequate precision value of 29.7534 shows an appropriate signal.

Regression model for DOP in terms of current and welding speed is presented by Eq. 1.

$$\begin{aligned}\mathrm{DOP} = {} & +5.93943 - 0.029236 \times \mathrm{Current} - 1.71310 \\ & \times \mathrm{WeldingSpeed} + 0.003500 \times \mathrm{Current} \\ & \times \mathrm{WeldingSpeed} + 0.000185 \times \mathrm{Current}^2 \\ & +0.144138 \times \mathrm{WeldingSpeed}^2\end{aligned} \tag{1}$$

A comparison of actual versus values predicted by the regression model is given in Fig. 4a. Variation of DOP with current and welding speed is shown in Fig. 4b. An increase in welding current from 80 to 120 A increased the DOP from 1.22 to 2.48 mm at constant welding speed(s). Similarly, a decrease in welding speed from 5 – 3 mm/s increased the DOP in the range of 1.22–2.48 mm. The DOP has an opposite variation trend with welding current and welding speed. The results are in accordance with the

Table 5 ANOVA table of full quadratic model for depth of penetration in TIG Welding for SS202

Source	Sum of Squares	DOF	Mean Square	F-value	p-value	Cont. %	Remarks
Model	1.54	5	0.3079	75.21	< 0.0001	98.09	Significant
A-Current	1.14	1	1.14	279.45	< 0.0001	72.61	
B-Welding Speed	0.2646	1	0.2646	64.63	< 0.0001	16.85	
AB	0.0196	1	0.0196	4.79	0.0649	1.25	
A^2	0.0152	1	0.0152	3.71	0.0955	0.97	
B^2	0.0574	1	0.0574	14.02	0.0072	3.66	
Residual	0.0287	7	0.0041			1.83	
Lack of Fit	0.0139	3	0.0046	1.26	0.3995	0.89	Not significant
Pure Error	0.0147	4	0.0037			0.94	
Cor Total	1.57	12				100	
Std. Dev.		0.064		**R^2**			0.9817
Mean		1.82		**Adjusted R^2**			0.9687
CV %		3.51		**Predicted R^2**			0.9186
				Adeq Precision			29.7534

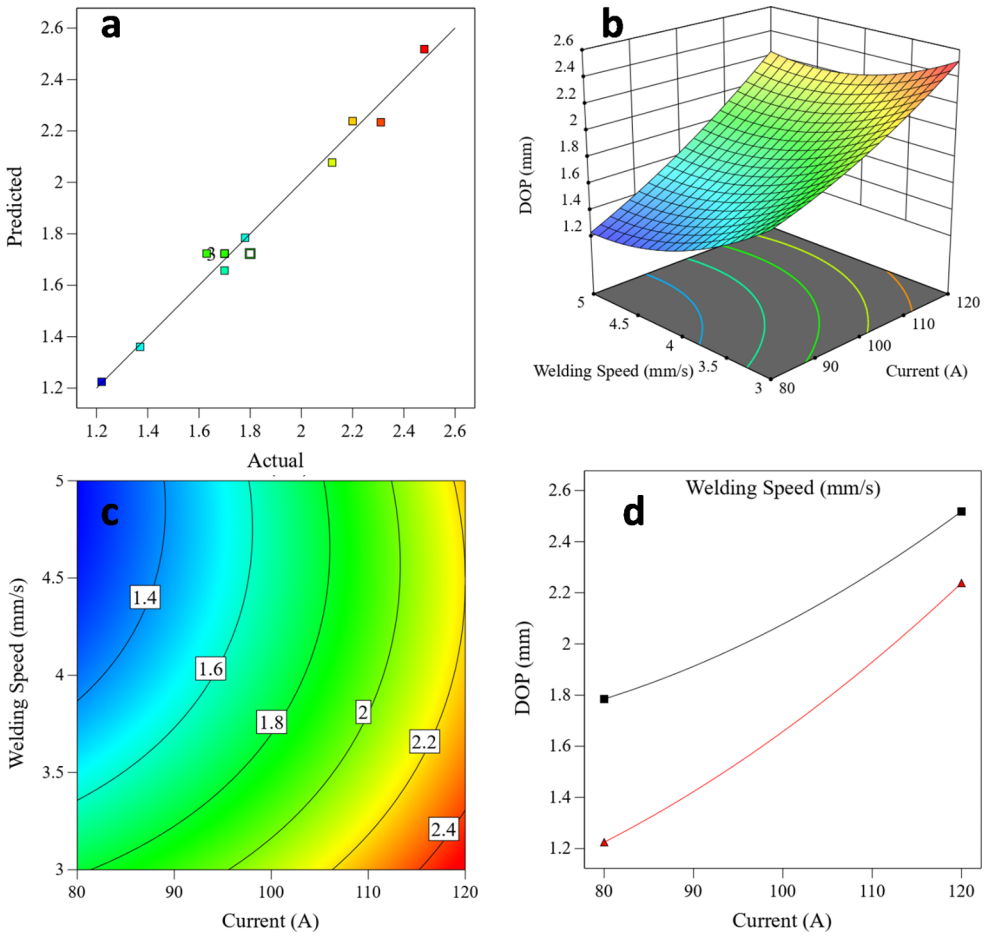

Fig. 4 Variation of DOP with welding parameters (**a**) comparison of actual and values predicted values (**b**) 3D response surface graph showing the variation of DOP with welding current and speed, (**c**) Contour plot, and (**d**) interaction plot

percentage contribution for change in DOP, where welding current had a more dominating effect than welding speed. Higher welding current and lower welding speed cause greater weld heat input, causing enhanced digging action of weld arc force; hence deeper is the penetration depth. The contour plot of DOP is presented in Fig. 4c, which shows the possible combinations of current and welding speed for constant DOP and can be used to determine the possible combinations for a particular value of DOP. Figure 4d shows the interaction effect between parameters and is insignificant except for the curvature effect of welding speed.

3.2.2 Weld width

As demonstrated in Table 6 for the ANOVA of the full quadratic model for weld width, A and B are crucial model terms. Non-significant lack of fit indicates that the model can be fitted. The current contributes 80.67% to weld width, whereas welding speed significantly contributes (12.56%) in total variation.

Adjusted R^2 of 0.9217 agrees fairly with the Predicted R^2 of 0.9002, as there is a discrepancy of less than 0.2. The signal-to-noise ratio is measured with sufficient accuracy. It is preferable to have a ratio higher than 4. Precision ratio of 26.3864 suggests that the signal is adequate. Regression model for weld width in terms of current and welding speed is presented in Eq. 2.

$$\begin{aligned}\text{WeldWidth} &= +1.88821 + 0.034667 \\ &\times \text{Current} - 0.273333 \times \text{WeldingSpeed}\end{aligned} \tag{2}$$

A comparison of actual versus values predicted by the regression model is presented in Fig. 5a. Variation of weld width with current and welding speed is shown in Fig. 5b. The change in welding current from 80 to 120 A increased the weld width for all welding speeds, while the change in welding speed from 3 to 5 mm/s decreased the weld width for all welding currents. Thus, weld width also had a similar variation trend with input parameters to that of DOP. The increase in weld width with welding current is due to the spread of the welding arc owing to higher welding heat. Faster welding speed causes lower heat input to weld so as the narrow weld, i.e., small weld width owing to the formation of the small weld pool. Welding current dominates the welding speed governing the weld width as suggested by percentage contribution. The contour plot is shown in Fig. 5c since it is a linear model, so there is no interaction (curvature) effect, as shown in Fig. 5d.

3.2.3 Weld bead hardness

It is evident from Table 7 that A, B, A^2, and B^2 are significant model terms. Welding speed (A) has a contribution of 62.03%, whereas welding current (B) has a 10.22% contribution. The percentage contribution of A^2 is even more than that of weld current and amounts to 25.52%. B^2 was also found to be significant but only contributed to 2.61%. The predicted R^2 of 0.9105 is in reasonable agreement with the adjusted R^2 of 0.9738. Adequate precision of 32.7345 indicates an adequate signal.

The regression model for weld bead hardness in terms of current and welding speed is presented in Eq. 3.

$$\begin{aligned}\text{WeldBeadHardness} &= -63.94253 + 8.01523 \\ &\times \text{Current} - 13.85632 \times \text{WeldingSpeed} - 0.1 \\ &\times \text{Current} \times \text{WeldingSpeed} - 0.039784 \\ &\times \text{Current}^2 + 5.08621 \times \text{WeldingSpeed}^2\end{aligned} \tag{3}$$

Predicted values of weld bead hardness are close to experimental ones, as evident from Fig. 6a. Figure 6b shows the variation of weld bead hardness with current and welding speed. Weld bead hardness first increases to the highest value at the mid-welding current. Further, increasing the welding current beyond mid-value decreases the weld bead hardness noticeably. Conversely, weld bead hardness increases with increased welding speed from 3 to 5 mm/s. From Fig. 6b, it is clear that welding speed has a more dominant influence on weld bead hardness than welding current. As shown in Table 7, welding speed contributes 62.03% to improve the weld bead hardness, whereas welding current only has a small contribution of 10.22%. The welding current governs heat generation while welding speed controls the heat input per unit length of the weld during welding. Faster welding speed and low current result in low heat input to weld, leading to faster cooling rate, low peak temperatures, and duration; hence, the chances of grain coarsening are lesser.

Table 6 ANOVA table of full quadratic for weld width in TIG welding for SS202

Source	Sum of Squares	DOF	Mean Square	F-value	p-value	Cont.%	Remarks
Model	3.33	2	1.67	71.63	< 0.0001	93.28	Significant
A-Current	2.88	1	2.88	123.98	< 0.0001	80.67	
B-Welding Speed	0.4483	1	0.4483	19.27	0.0014	12.56	
Residual	0.2326	10	0.0233			6.52	
Lack of Fit	0.086	6	0.0143	0.3907	0.8541	2.41	Not significant
Pure Error	0.1467	4	0.0367			4.11	
Cor Total	3.57	12				100	
Std. Dev.		0.1525		**R^2**			0.9347
Mean		4.26		**Adjusted R^2**			0.9217
CV %		3.58		**Predicted R^2**			0.9002
				Adeq Precision			26.3864

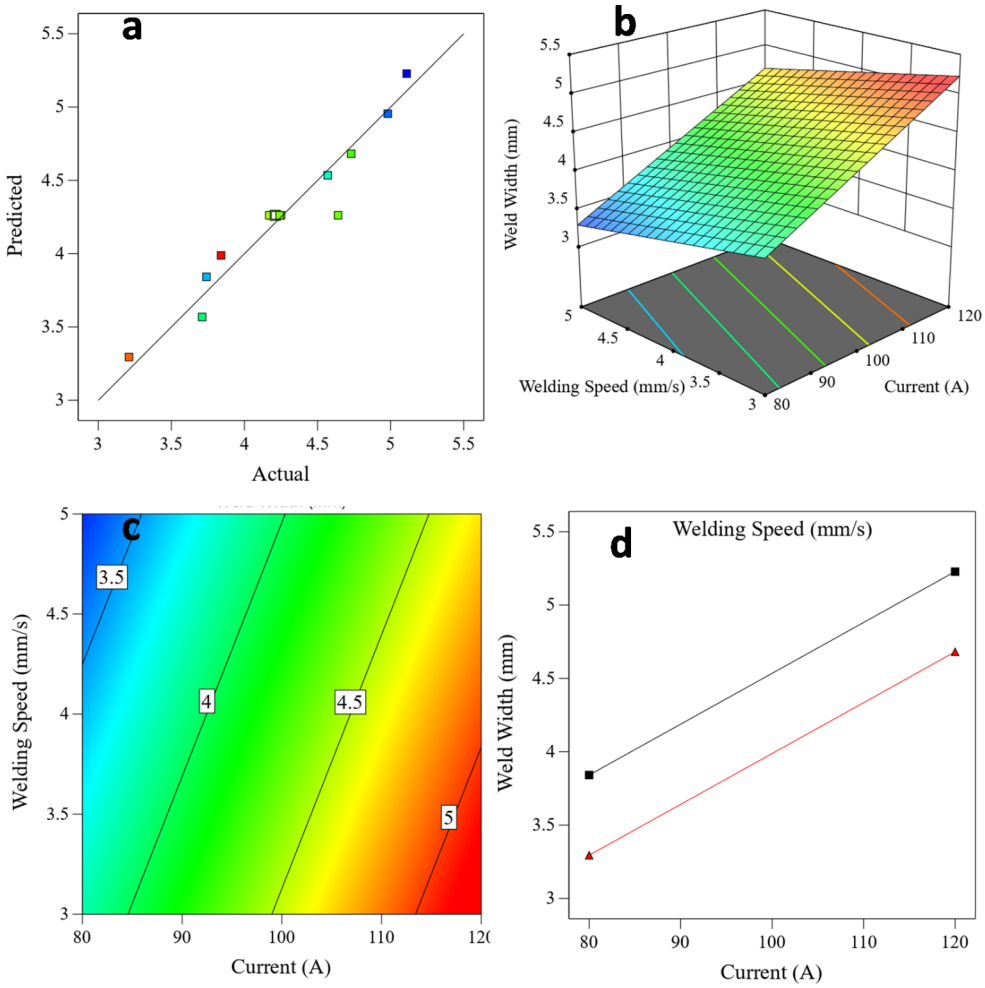

Fig. 5 Variation of weld width with welding parameters (**a**) comparison of actual and values predicted values (**b**) 3D response surface graph showing the variation of DOP with welding current and speed, (**c**) Contour plot, and (**d**) interaction plot

Table 7 ANOVA table for full quadratic Weld bead hardness in TIG Welding for SS202

Source	Sum of Squares	DOF	Mean Square	F-value	p-value	Cont. %	Remarks
Model	2698.86	5	539.77	90.16	< 0.0001	98.47	Significant
A-Current	280.17	1	280.17	46.8	0.0002	10.22	
B-Welding Speed	1700.17	1	1700.17	283.98	< 0.0001	62.03	
AB	16	1	16	2.67	0.1461	0.58	
A^2	699.45	1	699.45	116.83	< 0.0001	25.52	
B^2	71.45	1	71.45	11.93	0.0106	2.61	
Residual	41.91	7	5.99			1.53	
Lack of Fit	32.71	3	10.9	4.74	0.0834	1.19	Not significant
Pure Error	9.2	4	2.3			0.34	
Cor Total	2740.77	12				100	
Std. Dev.		2.45		**R^2**			0.9847
Mean		320.69		**Adjusted R^2**			0.9738
CV %		0.763		**Predicted R^2**			0.9105
				Adeq Precision			32.7345

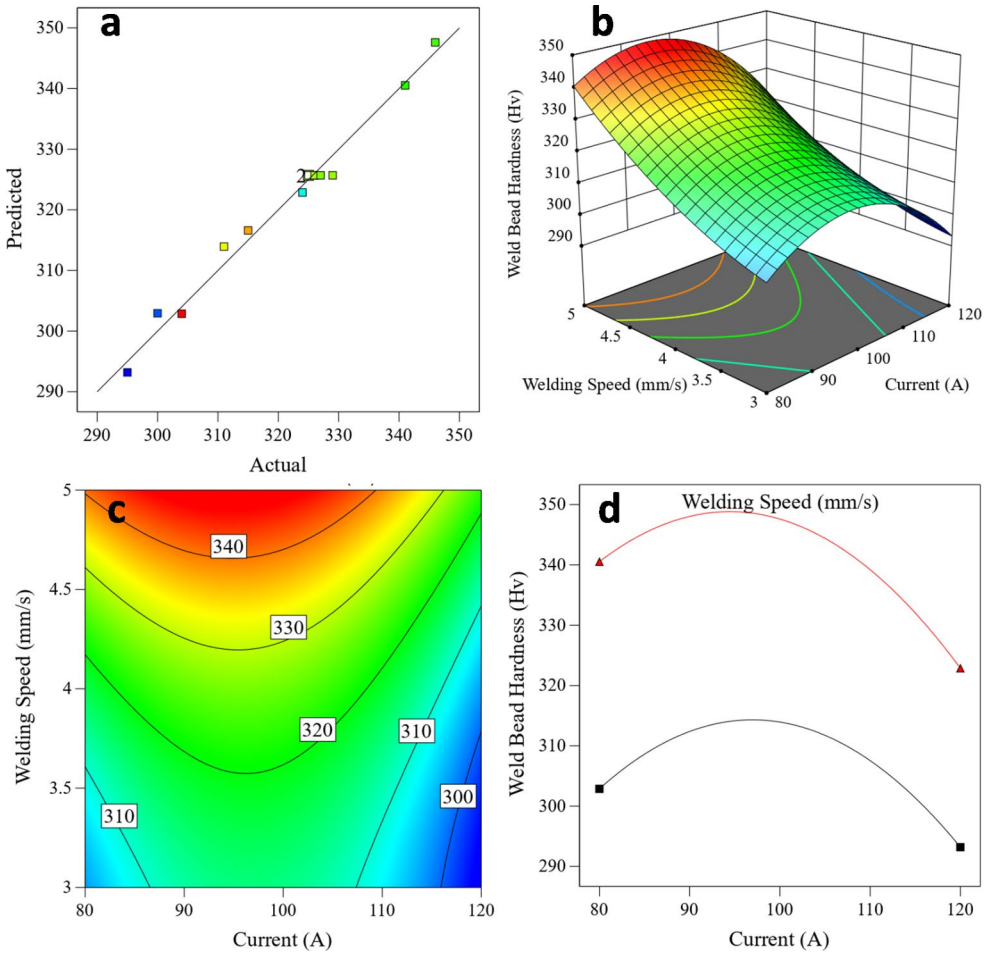

Fig. 6 Variation of weld bead hardness with welding parameters (**a**) comparison of actual and values predicted values (**b**) 3D response surface graph showing the variation of DOP with welding current and speed, (**c**) Contour plot, and (**d**) interaction plot

Table 8 ANOVA table for full quadratic HAZ hardness in TIG Welding for SS202

Source	Sum of Squares	DOF	Mean Square	F-value	p-value	Cont.%	Remarks
Model	1313.89	5	262.78	169.12	< 0.0001	99.18	Significant
A-Current	937.5	1	937.5	603.37	< 0.0001	70.77	
B-Welding Speed	28.17	1	28.17	18.13	0.0038	2.13	
AB	182.25	1	182.25	117.29	< 0.0001	13.76	
A^2	140.04	1	140.04	90.13	< 0.0001	10.57	
B^2	0.0402	1	0.0402	0.0259	0.8767	0	
Residual	10.88	7	1.55			0.82	
Lack of Fit	8.88	3	2.96	5.92	0.0594	0.67	Not significant
Pure Error	2	4	0.5			0.15	
Cor Total	1324.77	12				100	
Std. Dev.		1.25		**R^2**			0.9918
Mean		300.69		**Adjusted R^2**			0.9859
CV %		0.4145		**Predicted R^2**			0.9297
				Adeq Precision			45.4635

Moreover, the cooling rate also increases when weld heat input is decreased. Thus, owing to faster weld cooling, the extent of coarsening forming finer grains improves weld hardness. On the other hand, a slower weld cooling rate forms large columnar grains with widely spaced dendrites, resulting in lower weld hardness [23, 24]. Figure 6c and d show the contour and interaction plot, respectively.

3.2.4 HAZ hardness

Table 8 shows that A, B, AB, and A^2 are significant model terms, and the lack of fit is insignificant. Predicted R^2

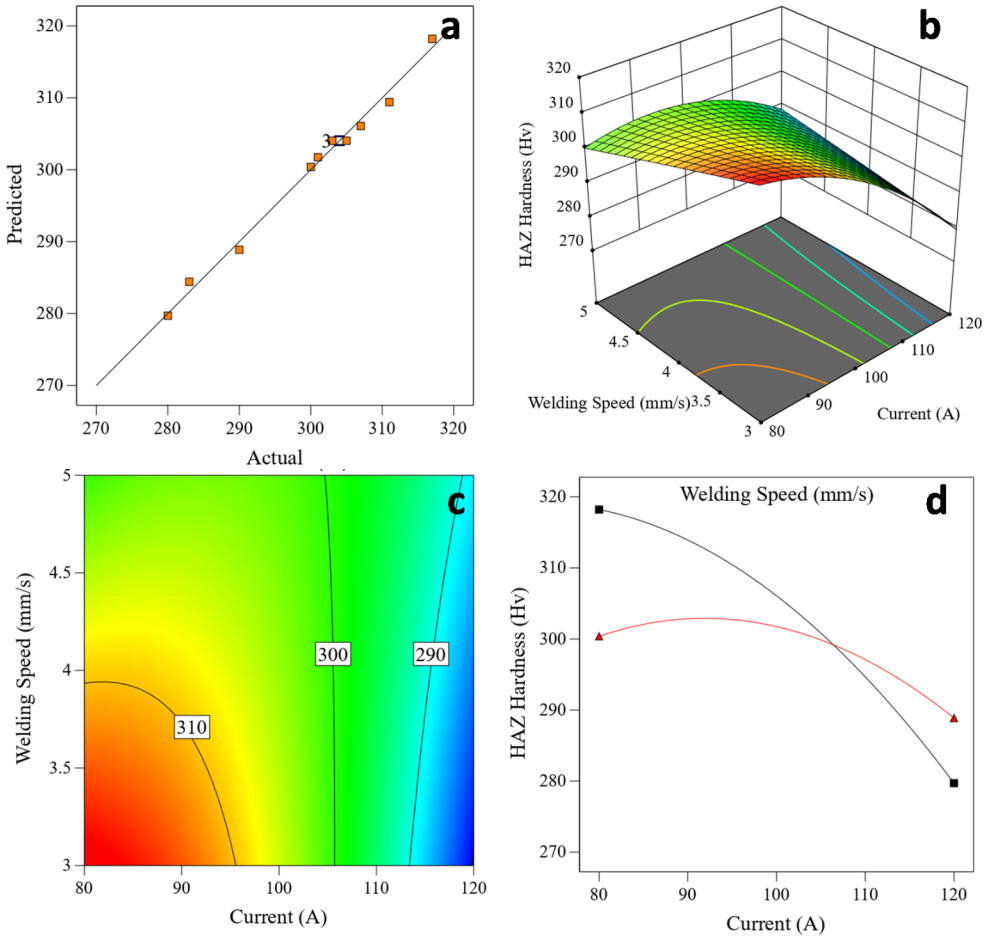

Fig. 7 Variation of HAZ hardness with welding parameters (**a**) comparison of actual and values predicted values (**b**) 3D response surface graph showing the variation of DOP with welding current and speed, (**c**) Contour plot, and (**d**) interaction plot

of 0.9297 is in fair agreement with the adjusted R^2 of 0.9859. Adequate precision measures the signal-to-noise ratio. Current has a 70.77% contribution in increasing the HAZ region's hardness, whereas welding speed only contributes to 2.13% in determining the HAZ hardness. Regression model in terms of current and welding speed is presented in Eq. 4.

$$\begin{aligned}\text{HAZHardness} = {} & +330.25287 + 1.58534 \\ & \times \text{Current} - 34.95115 \times \text{WeldingSpeed} + 0.3375 \\ & \times \text{Current} \times \text{WeldingSpeed} - 0.017802 \\ & \times \text{Current}^2 - 0.12069 \times \text{WeldingSpeed}^2\end{aligned} \tag{4}$$

It is evident from Fig. 7a that predicted values are close to experimental ones. The variation of HAZ hardness with current and welding speed is shown in Fig. 7b. HAZ hardness decreases with increased welding current and welding speed owing to coarsening, except for a rise in welding speed from 3 to 5 mm/s at a high-level constant welding current of 120 A. Welding current had a more significant role (70.77%) in controlling the HAZ hardness than welding speed (2.13%). The contour plot for the same is shown in Fig. 7c. The interaction of A (current) and B (welding speed) can be realized from Fig. 7d, which also justifies the higher percentage contribution of AB during ANOVA. It signifies that not only A and B but the interaction of A and B also affects the outcome, i.e., HAZ hardness depends on the current and welding speed levels.

Table 9 Criteria for Optimal Parameters

Input Parameters	Units	Goal	Limit	
			Lower	Upper
Current	A	In range	80	120
Welding Speed	mm/sec	In range	3	5
DoP	mm	Maximum	1.22	2.48
Weld Width	mm	Minimum	3.21	5.11
Weld Bead Hardness	Hv	Maximum	295	346
HAZ Hardness	Hv	Maximum	280	317

3.3 Confirmation test

Optimal parameters were determined by keeping input parameters in the prescribed range and maximizing or minimizing output parameters, as shown in Table 9. In the responses, DOP was set as a maximum to achieve maximum weld penetration, whereas weld width was set

Table 10 Optimal parameters for optimization

No.	Current	Welding Speed	DOP	Weld Width	Weld Bead Hardness	HAZ Hardness	Desirability	Remarks
1	**102.661**	**5**	**1.726**	**4.08**	**346.152**	**300.856**	**0.592**	**Selected**
2	102.826	5	1.73	4.086	346.043	300.792	0.592	
3	102.498	5	1.722	4.075	346.258	300.918	0.592	
4	89.705	3	1.908	4.178	312.214	314.103	0.537	
5	89.85	3	1.91	4.183	312.297	314.016	0.537	
6	90.772	3	1.924	4.215	312.785	313.446	0.537	

Table 11 Confirmation Test

(I = 103 A and S = 5 mm/sec)	Experimental mean	Predicted values	Error %
DoP	1.764	1.726	-2.15
Weld Width	4.097	4.08	-0.41
Weld Bead Hardness	347.216	346.152	-0.31
HAZ Hardness	302.614	300.856	-0.58

as a minimum to increase the aspect ratio. Weld bead and HAZ hardness were set to maximum to improve mechanical properties after welding.

Optimal process parameters are highlighted with a desirability of 0.592 in Table 10. The optimal value of input parameters, viz. welding current and welding speed, was ~ 103 A and 5 mm/sec.

The confirmation test was run on the parametric combination chosen from the best set of parameters. Three experimental trials were conducted for the confirmation test, and the average values were compared with the anticipated outcomes. The error percentage represents the discrepancy between the experimental mean and the expected result. Table 11 clarifies that the projected values closely match the experimental findings because the error percentage is so small.

4 Conclusions

Bead-on-plate welding was performed on SS202 plates using the TIG technique. Selected input variables greatly influenced the output variable with varying degrees. Welding current was more (72.61%) dominant in improving DOP than welding speed (16.85%). DOP was discovered to have a direct correlation with welding current and reciprocally with welding speed; higher welding current and slow welding speed result in increased DOP. Weld width had a similar trend of variation with welding current and speed to that of DOP. Faster welding speed and low welding current causes the minimum spread of weld, i.e., narrow weld. Bead hardness had a different trend of variation with welding current and speed and was found first to increase with welding current up to mid-level beyond which it decreases. However, it increases continuously with welding speed. Welding speed was more effective (62.03%) in controlling bead hardness than welding current (10.22%). Increase in welding current and speed are observed to cause a drop in HAZ hardness. Welding current had a more (70.77%) significant role in controlling the HAZ hardness than welding speed (2.13%). The predicted and experimental results are in close agreement with each other, as confirmed by the confirmation experiment.

References

1. Urde, V.P., Ambade, S.P.: An overview of Welded Low Nickel Chrome-Manganese Austenitic and Ferritic Stainless Steel. J. Mater. Sci. Eng. **05** (2016). https://doi.org/10.4172/2169-0022.1000231
2. Durgutlu, A.: Experimental investigation of the effect of hydrogen in argon as a shielding gas on TIG welding of austenitic stainless steel. **25**, 19–23 (2004). https://doi.org/10.1016/j.matdes.2003.07.004
3. Mishra, R.R., Tiwari, V.K.: A study of tensile strength of MIG and TIG welded dissimilar joints of mild steel and stainless steel. Int. J. Adv. Mater. Sci. Eng. **3**, 23–32 (2014). https://doi.org/10.14810/ijamse.2014.3203
4. Sharma, C., Upadhyay, V.: Friction stir welding of dissimilar aluminum alloys AA5086 and AA7039. J. Phys. Conf. Ser. **1240** (2019). https://doi.org/10.1088/1742-6596/1240/1/012160
5. Mishra, R.S., Ma, Z.Y.: Friction stir welding and processing. 50, 1–78 (2005). https://doi.org/10.1016/j.mser.2005.07.001
6. Sharma, C., Upadhyay, V.: Microstructure and mechanical behavior of similar and dissimilar AA2024 and AA7039 friction stir welds. Eng. Rev. **41**, 21–33 (2020). https://doi.org/10.30765/ER.1533
7. Taiwade, R.V., Patre, S.J., Patil, A.P.: Studies on welding and sensitization of chrome-manganese austenitic stainless steel. Trans. Indian Inst. Met. **64**, 513–518 (2011). https://doi.org/10.1007/S12666-011-0077-6
8. Krishnan, S., Kulkarni, D.V., De, A.: Multipass pulsed current gas metal arc welding of P91 steel. Sci. Technol. Weld. Join. **21**, 171–177 (2016). https://doi.org/10.1179/1362171815Y.0000000080
9. Sambherao, A., Www, W., Sambherao, A.B.: Use of activated flux for increasing penetration in austenitic stainless steel while performing GTAW. Int. J. Emerg. Technol. Adv. Eng Accessed: Jun. 18, 2020. [Online]. Available: (2013). https://www.researchgate.net/publication/271766098
10. Li, D., Lu, S., Li, D., Li, Y.: Principles giving high penetration under the double shielded TIG process. J. Mater. Sci. Technol. **30**, 172–178 (2014). https://doi.org/10.1016/j.jmst.2013.09.002
11. Wang, L.L., Lu, F.G., Cui, H.C., Tang, X.H.: Investigation on thermal inertia of GMAW-P welding on Al alloy. Sci. Technol.

Weld. Join. **20**(2), 106–114 (2015). https://doi.org/10.1179/1362171814Y.0000000260
12. Sharma, N., Abduallah, W.S., Garg, M., Gupta, R.D., Khanna, R., Sharma, R.C.: Optimization of TIG welding parameters for the 202 stainless steel using NSGA-II. J. Eng. Res. **8**, 206–221 (2020). https://doi.org/10.36909/JER.V8I4.7071
13. Gopinath, V., Manojkumar, T., Sirajudeen, I., Yogeshwaran, S., Chandran, V.: Optimization of process parameters in TIG welding of AISI 202 stainless steel using response surface methodology. Int. J. Appl. Eng. Res. **10**, 11053–11057 (2015)
14. Saha, M., Dhami, S.S.: Effect of TIG Welding parameter of Welded Joint of Stainless Steel SS304 by Trends in Mechanical Engineering & Technology Effect of TIG Welding parameter of Welded Joint of Stainless Steel SS304 by TIG Welding. (2019). https://doi.org/10.2139/ssrn.3643709
15. Verma, V., Singh, A., Pandey, A.K., Sharma, C., Sonia, P., Saxena, K.K.: Experimental investigation of tensile properties and microstructure of TIG welded dissimilar joints of Al6061/Al5083 Aluminium alloy. Indian J. Eng. Mater. Sci. **29**, 262–270 (2022). https://doi.org/10.56042/ijems.v29i2.46110
16. Lakshminarayanan, A.K., Balasubramanian, V., Elangovan, K.: Effect of welding processes on tensile properties of AA6061 aluminium alloy joints. Int. J. Adv. Manuf. Technol. **40**, 286–296 (2009). https://doi.org/10.1007/s00170-007-1325-0
17. Ogedengbe, T.I., Abioye, T.E., Ekpemogu, A.I.: Investigation of mechanical properties and parametric optimization of the dissimilar GTAW of AISI 304 stainless steel and low carbon steel. World J. Eng. **15**, 584–591 (2018). https://doi.org/10.1108/WJE-12-2017-0412
18. Vidyarthy, R.S., Kulkarni, A., Dwivedi, D.K.: Study of microstructure and mechanical property relationships of A-TIG welded P91–316L dissimilar steel joint. Mater. Sci. Eng. A. **695**, 249–257 (2017). https://doi.org/10.1016/j.msea.2017.04.038
19. Babbar, A., Kumar, A., Jain, V., Gupta, D.: Enhancement of activated tungsten inert gas (A-TIG) welding using multi-component TiO2-SiO2-Al2O3 hybrid flux. Meas. J. Int. Meas. Confed. **148** (2019). https://doi.org/10.1016/j.measurement.2019.106912
20. Baghel, A., Sharma, C., Rathee, S., Srivastava, M.: Influence of activated flux on micro-structural and mechanical properties of AISI 1018 during MIG welding. Mater. Today Proc. **47**, 6947–6952 (2020). https://doi.org/10.1016/J.MATPR.2021.05.210
21. Baghel, A., Sharma, C., Rathee, S., Srivastava, M.: Activated flux TIG welding of dissimilar SS202 and SS304 alloys: Effect of oxide and chloride fluxes on microstructure and mechanical properties of joints. Mater. Today Proc. 47, 7189–7195 (2020). https://doi.org/10.1016/j.matpr.2021.07.199
22. Kumar, R., Upadhyay, V., Sharma, C.: Modeling and optimization of process parameters for friction stir welding of dissimilar aerospace alloys AA2014 and AA7075. Eng. Rev. **42**, 59–78 (2022). https://doi.org/10.30765/ER.1778
23. Kolhe, K.P., Datta, C.K.: Prediction of microstructure and mechanical properties of multipass SAW. **7**, 241–249 (2007). https://doi.org/10.1016/j.jmatprotec.2007.06.066
24. Khoshroyan, A., Darvazi, A.R.: Effects of welding parameters and welding sequence on residual stress and distortion in Al6061-T6 aluminum alloy for T-shaped welded joint. Trans. Nonferrous Met. Soc. China. **30**, 76–89 (2020). https://doi.org/10.1016/S1003-6326(19)65181-2